Analysis and Design of an Embedded Antenna for Concrete Wireless Monitoring Applications

***Abstract*—We propose an embedded circularly-polarized antenna for battery-less sensor monitoring of concrete structures. In particular, we focus our effort in designing a patch antenna able to work in concrete with different dielectric properties while still keeping unchanged impedance to guarantee an optimal power transfer. To this aim, the antenna is designed and optimized by exploiting both an analytical and a full wave numerical approach. The results give physical insight into the antenna performance and explains the robustness (against concrete variations) of the antenna. Experimental measurements fully confirm the model predictions.**

***Index Terms*—Concrete structure monitoring, embedded sensors, patch antennas model, circular polarization, wireless power transmission.**

I. Introduction

COMMUNICATION by backscattered power was first proposed in 1948 [1] and in the recent years the idea has been extended to wireless sensors and wireless sensor networks. This technology keeps on spreading in many areas and also in applications where it is not possible to provide battery or local power for electronics. As a result, remotely powered sensor may represent effective smart solutions. However, they require an efficient power transmission from the antenna to the integrated circuit (IC) and then an accurate design of the antenna input impedance.

In structural health monitoring (SHM) of concrete [2], embedded battery-less sensors are employed for wireless energy and data transfer between sensors (f.i. pressure sensors) and an external reader. Of course, the antenna must be properly designed according to the background medium. Antennas embedded in (possibly lossy) media have been investigated in different area ranging from submarine [3] to biomedical applications [4], [5], and wireless through-wall communications [6]. However in SHM of concrete structures [2], since the concrete's permittivity and loss tangent may change depending on the concrete lifetime, internal state and type, the goal is to minimize the influence of the background material on the antenna performance.

In the last years a great interest has been shown in the wireless SHM of infrastructures, such as buildings or bridges. To this aim several approaches have been followed to achieve effective solutions in antenna designing. In [7] a λ_0- and $4\lambda_0$-thick foam cover was used to mitigate the effect of the concrete on the antenna performance. In [8] the same approach exploiting a vacuum smaller box has been followed where the concrete being closer to the antenna and has the effect to reduce the resonant length. In [9] a quite complicated cavity-backed antenna is proposed.

In the present work our focus is on the design and the optimization of "robust" antennas against the concrete variations [2]. In some sense, the goal is concerned with the design of an antenna with a large "permittivity bandwidth". In particular, the antenna is assumed to work in a given range of complex permittivity values, which are $[4-9]$ and $[0-0.3]$ for the permittivity and the loss tangent, respectively. These values are typical dielectric parameters for the concrete, [10]. Such a wide variation is expected to hugely affect both the antenna input impedance and the gain. We assume as working frequency 900 MHz, which is very close to the European and American standards (868 MHz or 915 MHz) and required bandwidth for data transmission is 10 MHz.

The paper is organized as follow. The antenna layout is described in section II. In section III we present an analytical model to evaluate the impedance of a rectangular patch antenna embedded in media with different permittivity values. In section IV we carry out a full-wave numerical study and discuss the antenna performance and section V we present experimental results for an antenna prototype embedded in a concrete block. Conclusion follow in section VI.

II. Antenna Layout

The project constrains assume the antenna positioned at 3 cm far from a flat concrete-air interface. The antenna layout is shown in Fig. 1. It consists of a metallic patch with a ground plane printed on a dielectric substrate with relative permittivity $\epsilon_{r\,s}$ = 9.8. The radiating patch dimension (l_x and l_y) has been chosen to achieve an operation frequency of 900 MHz. The antenna is assumed to be connected to a standard 50 Ω SMA connector, with inner and outer diameters d_0 and d respectively. Two dielectric "covers" with $\epsilon_{r\,c}$ are stacked over the patch and under the ground to protect the antenna metallization from the concrete. The dielectric materials used for the antenna are laminates TMM 10i and TMM6 from Rogers Corporation for substrate and protective layers, respectively. The above shielding method, compared to the air box adopted in [8], allows a smoother permittivity transition, and is simpler as well as less expensive than the solution chosen in [9].

This is the post-print of the following article: G. Castorina, L. Di Donato, A. F. Morabito, T. Isernia, and G. Sorbello, "Analysis and Design of a Concrete Embedded Antenna for Wireless Monitoring Applications," IEEE Antennas and Propagation Magazine, vol. 58, n. 6, pp. 76-93, 2016. Article has been published in final form at: https://ieeexplore.ieee.org/document/7762866. DOI: 10.1109/MAP.2016.2609818.

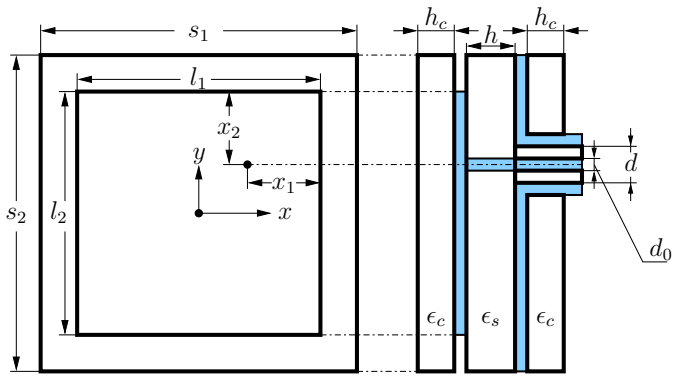

Fig. 1. Antenna layout. Frontal and lateral view with cut at probe feed. Metal layers in blue (color online).

TABLE I
ANTENNA PARAMETERS

Parameters	l_1	l_2	$x_{1,2}$	$s_{1,2}$	h_c	h	d_0	d
Value [mm]	49.6	47.6	10	60	2.54	3.175	0.9	2.98

III. ANALYTICAL MODEL

An antenna embedded in a dielectric medium with relative permittivity ϵ_{rb} changes the input impedance according to the following identity [11]:

$$Z_{\text{in}}(f;\epsilon=\epsilon_0\epsilon_{rb}) = \frac{Z_{\text{in}}(f\sqrt{\epsilon_{rb}};\epsilon=\epsilon_0)}{\sqrt{\epsilon_{rb}}}, \tag{1}$$

i.e. the input impedance of the embedded antenna is equal to the impedance of the same antenna in air ($\epsilon=\epsilon_0$) at frequency $f\sqrt{\epsilon_{rb}}$ scaled by $1/\sqrt{\epsilon_{rb}}$.

A wideband antenna is therefore only partially synonymous of wide dielectric bandwidth. An example is any self-complementary antenna [12] with input impedance ideally independent from frequency [12, eq. (10)]:

$$Z_{\text{in}} = \frac{Z_0}{2} \tag{2}$$

but dependent on the medium intrinsic impedance, Z_0, and therefore on the background relative permittivity ϵ_{rb}.

The proposed patch antenna input impedance will not follow the identity (1) as the antenna is composed by several dielectric layers in order to mitigate the influence of the background medium on the antenna input impedance.

In this section we present an extended analytical model to evaluate the input impedance of a rectangular patch antenna embedded in a given medium (not necessarily air). The model takes into account two resonances due to the presence of two orthogonal modes needed to achieve circular polarization.

Each of the two resonances can be modeled by an RLC parallel circuit with two slightly different resonant frequencies, f_1 and f_2 (from this point the 1 subscript refers to the first resonance, TE_{10}, along x-axis and 2 to the second one, TE_{01}, along y-axis). Since the voltage at the probe coordinates is due to the sum of the TE_{10} and TE_{01} modes, the equivalent circuit for the input impedance is given by the series of the two parallel RLC circuit [13]. An extra inductance associated to the probe feed can be modeled by series inductor X_{feed}.

The input impedance of the circularly polarized antenna is equal to:

$$Z_{\text{in}}(f) = jX_{\text{feed}} + Z_{\text{in},1} + Z_{\text{in},2} \tag{3}$$

wherein X_{feed} [14], [15, (1)] can be eventually neglected and Z_1 and Z_2 are the impedances of the two RLC parallel circuits [13]:

$$Z_{1,2}(f) = \frac{R_{1,2}}{1+Q_{1,2}^2\left(\frac{f}{f_{1,2}}-\frac{f_{1,2}}{f}\right)^2} + \\ - j\frac{R_{1,2}Q_{1,2}\left(\frac{f}{f_{1,2}}-\frac{f_{1,2}}{f}\right)}{1+Q_{1,2}^2\left(\frac{f}{f_{1,2}}-\frac{f_{1,2}}{f}\right)^2} \tag{4}$$

In (4) we need to specify the resonant frequencies, $f_{1,2}$, the quality factors $Q_{1,2}$ and the resonant resistances $R_{1,2}$ for the embedding medium permittivity.

A. Resonant frequency

The resonant frequencies, $f_{1,2}$, can be evaluated with the well know equation [16, eq. (14.5)]:

$$f_{1,2} = \frac{c_0}{2\sqrt{\varepsilon_{\text{eff }1,2}}l_{\text{eff }1,2}} \tag{5}$$

where $\varepsilon_{\text{eff }1,2}$ is the effective permittivity of a microstrip line 1,2 of width $w_{1,2} = l_{2,1}$ (where l is the resonant length while w the corresponding strip width). To evaluate $\varepsilon_{\text{eff }1,2}$ the equation in [16, eq. (14.1)] has been generalized to take into account the medium permittivity, ε_{rb}:

$$\varepsilon_{\text{eff }1,2} = \frac{\varepsilon_{rs}+\varepsilon_{rb}}{2} + \frac{\varepsilon_{rs}-\varepsilon_{rb}}{2}\left(1+\frac{12}{\frac{w_{1,2}}{h}}\right)^{-\frac{1}{2}}. \tag{6}$$

In (5) the effective length, $l_{\text{eff }1,2}$, that takes into account the effect of the fringing fields and can be calculated as [17, (6)]:

$$l_{\text{eff }1,2} = l_{1,2} + \left(\frac{w_{\text{eq }1,2}-w_{1,2}}{2}\right)\frac{\varepsilon_{\text{eff }1,2}+0.3}{\varepsilon_{\text{eff }1,2}-0.258} \tag{7}$$

where, in turn, the equivalent width is given by the planar waveguide model [18, pag. 30], [19, eq. (3.85)] [20, § 3.14.1]:

$$w_{\text{eq }1,2} = \frac{h}{Z_{1,2}(\varepsilon_{rs})}\sqrt{\frac{\mu_0}{\varepsilon_{\text{eff }1,2}}} = \sqrt{\frac{\mu_0}{\epsilon_0}}\frac{h}{Z_{00}} \tag{8}$$

where $Z_{1,2}(\varepsilon_{rs})$ is the characteristic impedance of a microstrip line 1, 2 of width $w_{1,2} = l_{2,1}$ on a substrate of height h and dielectric permittivity ε_{rs} inside a background medium of dielectric permittivity ε_{rb} [14, eq. (10)], [21, eq. (2.124b)], [20, (43.180)]:

$$Z_{1,2}(\varepsilon_{rs}) = \frac{Z_{00}\left(\frac{w_{1,2}}{h}\right)}{\sqrt{\varepsilon_{\text{eff }1,2}}} \tag{9}$$

where Z_{00} is the, so called, characteristic impedance of the empty microstrip [20].

B. Quality factor

Quality factors, $Q_{1,2}$, for both resonant frequencies can be evaluated from [16, eq. (14.83)]:

$$Q_{1,2} = \left(\frac{1}{Q_{\text{rad}\,1,2}} + \frac{1}{Q_d} \right)^{-1} \tag{10}$$

where $Q_{\text{rad}\,1,2}$ are the losses due the radiation from the walls [22], [14, (14)]:

$$Q_{\text{rad}\,1,2} = \frac{c_0 \sqrt{\varepsilon_{\text{dyn}}}}{4 f_{1,2} h} \tag{11}$$

and Q_d is the quality factor due to dielectric losses

$$Q_d = \frac{1}{\tan \delta} \tag{12}$$

For high conductive metals (f.i. copper) conductor losses are negligible and, therefore, they may be neglected in this analytic model.

In equation (11) the dynamic permittivity $\varepsilon_{\text{dyn}} \approx \varepsilon_{rs}/\varepsilon_{rb}$ is used to take into account the fact that the patch is embedded into a variable background, with permittivity ε_{rb}, and to consider the effect of the fringing fields at the edges of the patch. The approach adopted in [14] has been extended to a generic embedding material with permittivity ε_{rb}, by defining

$$\varepsilon_{\text{dyn}} = \frac{C(\varepsilon_{rs})}{C(\varepsilon_{rb})} = \frac{C(\varepsilon_{rs})}{\varepsilon_{rb} C(\varepsilon_0)} \tag{13}$$

wherein the dynamic capacity in presence of a dielectric can be written as

$$C(\varepsilon_{rs}) = C_0(\varepsilon_{rs}) + 2C_{e1}(\varepsilon_{rs}) + 2C_{e2}(\varepsilon_{rs}) \tag{14}$$

where, in turn, $C_0(\varepsilon_{rs})$ is the capacity without the contribution of the fringing fields, and can be expressed as

$$C_0 = \frac{\varepsilon_{rs} \varepsilon_0 l_1 l_2}{h}. \tag{15}$$

The fringing fields are taken into account adding the edge capacitance $C_{e1}(\varepsilon_{rs})$ and $C_{e2}(\varepsilon_{rs})$ to C_0 [23]. The edge capacitance can be evaluated as:

$$\begin{aligned} C_{e1,2}(\varepsilon_{rs}) &= \frac{1}{2} \left[\frac{l_{1,2}}{v_{ph\,1,2} Z_{1,2}(\varepsilon_{rs})} - C_0(\varepsilon_{rs}) \right] \\ &= \frac{1}{2} \left[\frac{l_{1,2}\ \varepsilon_{\text{eff}\,1,2}}{c_0 Z_{00}} - \frac{\varepsilon_{rs} \varepsilon_0 l_1 l_2}{h} \right] \end{aligned} \tag{16}$$

where $v_{ph\,1,2}$ is the phase velocity and $Z_{1,2}(\varepsilon_{rs})$ is the microstrip line characteristic impedance given by (9). The above equations leads to:

$$C(\varepsilon_{rs}) = \frac{l_1 \varepsilon_{\text{eff}\,1}}{c_0 Z_{00}} + \frac{l_2 \varepsilon_{\text{eff}\,2}}{c_0 Z_{00}} - \frac{\varepsilon_{rs} \varepsilon_0 l_1 l_2}{h}. \tag{17}$$

In (13), $C(\varepsilon_{rb})$ can be evaluated replacing ε_{rs} and ε_{eff} with ε_{rb} in equations (14)-(16):

$$C(\varepsilon_{rb}) = \frac{l_1 \varepsilon_{rb}}{c_0 Z_{00}} + \frac{l_2 \varepsilon_{rb}}{c_0 Z_{00}} - \frac{\varepsilon_{rb} \varepsilon_0 l_1 l_2}{h}. \tag{18}$$

C. Resonant resistance

The resonant resistances, $R_{1,2}$, can be expressed [14, eq. (3)], [18, eq. (4.23c)]:

$$R_{1,2} = \frac{Q_{1,2}}{\pi f_{1,2}} \frac{h}{\varepsilon_{\text{dyn}} \varepsilon_{rb} \varepsilon_0 l_1 l_2} \cos^2 \left(\frac{\pi x_{\text{eff}\,1,2}}{l_{\text{eff}\,1,2}} \right) \tag{19}$$

where to take in account the effect of the fringing fields the edge-feed distance is corrected with [24]

$$x_{\text{eff}\,1,2} = x_{1,2} + \frac{l_{\text{eff}\,1,2} - l_{1,2}}{2} \tag{20}$$

considering the patch effective length (7).

D. Model validation

Full-wave simulations performed with Ansys HFSS are in good agreement with the model analytical results. Moreover, effective permittivity and characteristic impedance, eqs. (6) and (9), have been verified against numerical result for a wide range of dielectric properties of the substrate and of the embedding background by 2D simulations. The resonant frequency formula, eq. (5), has been verified by a full-wave 3D simulations. It can also be easily verified, by inspection of the equations, that the input impedance follows the general rule (1) in the case $\varepsilon_{rs} = \varepsilon_{rb}$.

The analytical input impedances, from (3), well match the simulated ones. In particular, the comparison for three cases of embedding medium ($\varepsilon_{rb} = 4, 6$ and 9) are shown in fig. 2

The simulated and analytical values of the antenna input impedance at 900 MHz are plotted in the range of interest, see fig. 3. The comparison shows a good agreement between the model and the simulations. The differences can be attributed to the approximation introduced in the model, as for example, the static nature of the model in eq. (6).

IV. Numerical Results

The analytical model does not consider a lossy background. Moreover, as described in section II, a box is introduced for a mechanical and chemical protection of the metal layers as well as to increase its performance against the embedding medium variations.

The comparison of $|S_{11}|$ curves for three different ε_{rb} values is shown in fig. 4 for the proposed antenna with covers (material and geometric details in section II). For each of these cases the $|S_{11}|$ of the proposed antenna is lower than -17 dB and the antenna is matched in the band of interest. The impedance curves on Smith chart are plotted in the inset of the same fig. 4, from which can be appreciated the huge benefic impact of the cover on the robustness of the antenna. These results confirm that the use of a box with a proper designed permittivity allows to achieve a good impedance matching in the frequency band of interest and for a wide permittivity range of the concrete. In particular, for this antenna, numerical simulation show that the permittivity band at -10 dB is enlarged from $5 \leq \varepsilon_{rb} \leq 9$ to $4 \leq \varepsilon_{rb} \leq 11$ using the covers.

Also the axial ratio (AR) is highly improved by the covers, see table II. For $\varepsilon_{rb} = 4$ and 9, the AR is lower than about 6 dB with covers and over 12 dB without them.

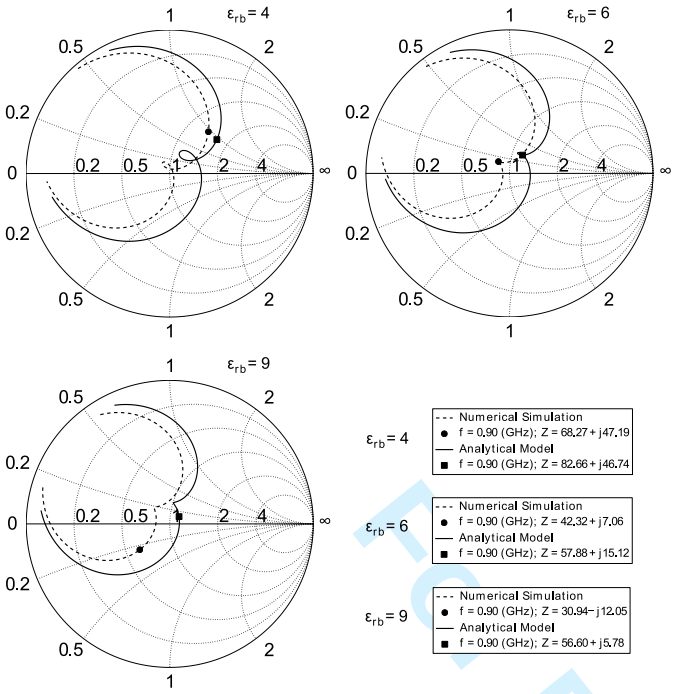

Fig. 2. Smith chart with analytical and simulated antenna input impedance for different embedding medium permittivity: $\varepsilon_{rb} = 4$, 6 and 9. Antenna without covers.

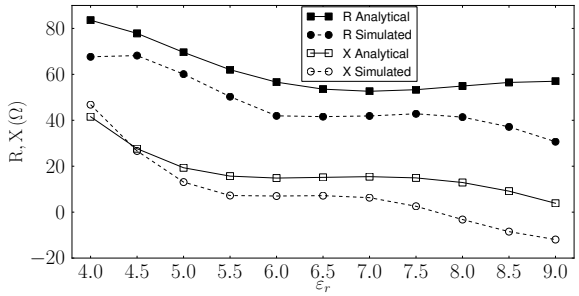

Fig. 3. Simulated and analytically computed real and imaginary part of the input impedance for the proposed antenna vs permittivity at 900 MHz.

A parametric study has been done to evaluate how the dimensions of the concrete block where antenna is embedded modify the antenna input impedance and radiation pattern. While the S_{11} is not significantly affected by the concrete dimensions radiation patterns can be influenced by dimensions and shape of the latter. In particular LHCP gains have been computed for the antenna embedded in concrete box with different dimension, and for a flat interface air-concrete of infinite extent. In the latter case the concrete semi-space was simulated with a MoM based solver. In the worst case LHCP gain is approximately -7 dB along the z axis and this power loss could be accounted for in the link budget.

V. Measurements

In this paragraph the experimental validation is presented. The antenna has been realized and embedded into a concrete

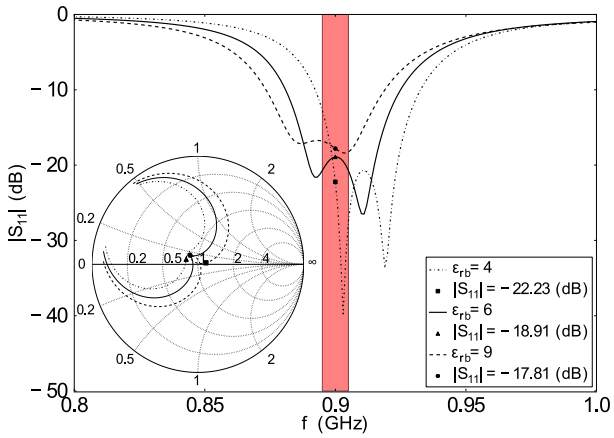

Fig. 4. Simulated S_{11} vs permittivity for the proposed antenna with covers. The frequency band of interest is highlighted. Inset: simulated input impedance on Smith chart. Infinite lossless background with concrete permittivity $\varepsilon_{rb} = 4, 6, 9$.

TABLE II
Simulated Axial Ratio in boresight direction. Infinite lossless background.

		$\varepsilon_{rb} = 4$	$\varepsilon_{rb} = 6$	$\varepsilon_{rb} = 9$
AR (dB)	No Covers	12.10	0.13	12.43
	Covers	6.13	0.49	4.61

block of side 15 cm, see fig. 5. The $|S_{11}|$ is in good agreement with the simulation's results as shown in fig. 6 and attains -19.9 dB at 900 MHz. A comparison of simulated and measured input impedance is shown on Smith chart in the inset of the same fig. 6. The slightly mismatch observed may be due to the difference between the dielectric properties used in the simulations and that of the actual concrete block (not measured).

The measured LHCP gain is shown in fig. 7 for a block of 15 cm, where it can be seen that for $\theta \in \pm 30°$ the LHCP gain is greater than -3 dB.

VI. Conclusion

A compact patch antenna for wireless monitoring applications of concrete buildings has been designed by means of an extended analytical model and numerical simulations. It shows a robust performance against permittivity variation of the embedding concrete thanks to a "region of guard" with a proper assigned permittivity. This approach allows to design in a simple way very stable antennas in terms input impedance and axial ratio. As a result, the antenna work for background permittivity values ranging from 4 to 11, while keeping substantially unchanged the $|S_{11}|$ at the frequency of 900 MHz. Interestingly, the LHCP gain is in the range $[-3, -0.6]$ dB over an arc of ± 30 with the maximum in the boresight direction. The overall results suggest the suitability of the proposed antenna for an efficient power transfer in wireless communications.

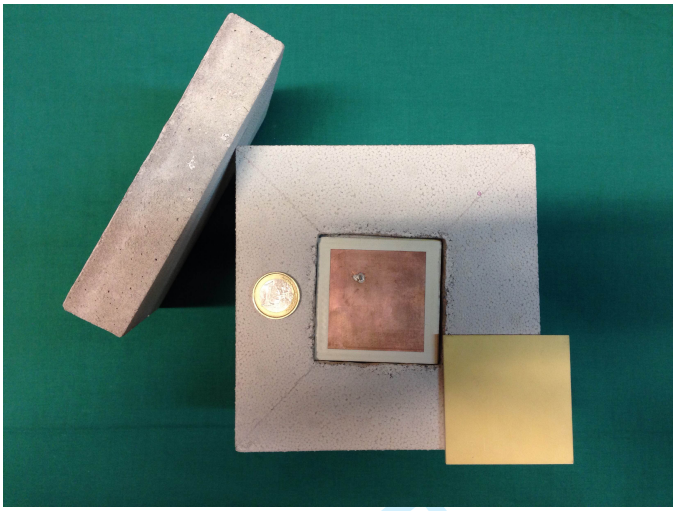

Fig. 5. The prototype antenna without the upper cover (shown on the right) embedded in the concrete block without the cap (3 cm thick) which simulates the interface (shown on the left).

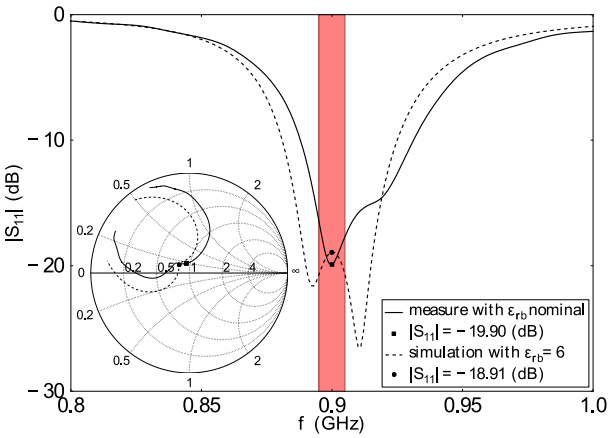

Fig. 6. Simulated and measured S_{11} for the proposed antenna in a cubic concrete block of side 15 cm. Frequency band of interest is highlighted. Inset: simulated and measured input impedance on Smith chart. Nominal concrete permittivity, used for simulation, $\varepsilon_{rb} = 6$; nominal concrete loss tangent, $\tan\delta = 0.03$.

VII. Acknowledgement

This work is partially supported by PON Smart Cities II, SMART CONCRETE SCN_00190 project. The authors wish to thank Ing. Mario Pavone for the support in the antenna realizations.

References

[1] H. Stockman, "Communication by means of reflected power," *Proceedings of the IRE*, vol. 36, no. 10, pp. 1196–1204, Oct 1948.

[2] (2014) Development of high performance, low cost technologies and efficient systems for internal structural monitoring and for safety implementation of concrete civil constructions and buildings. [Online]. Available: http://www.smartconcrete.org/

[3] R. W. P. King, G. S. Smith, M. Owens, and T. T. Wu, *Antennas in matter: Fundamentals, theory, and applications*. MIT, 1981, vol. 81.

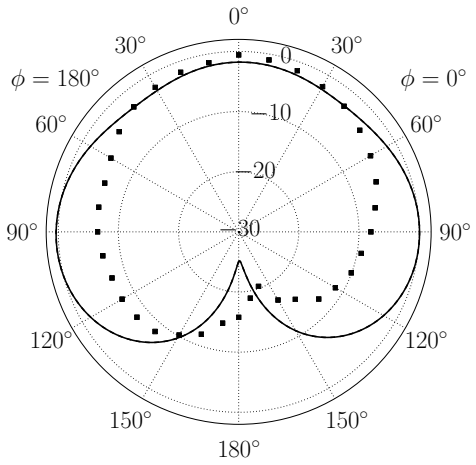

Fig. 7. Simulated (contiunos line) and measured (squares) LHCP gain for the proposed antenna in a cubic concrete block of side 15 cm.

[4] A. Kiourti and K. S. Nikita, "Miniature scalp-implantable antennas for telemetry in the MICS and ISM bands: Design, safety considerations and link budget analysis," *IEEE Trans. Antennas Propag.*, vol. 60, no. 8, pp. 3568–3575, 2012.

[5] C. Liu, Y. Guo, and S. Xiao, "Capacitively loaded circularly polarized implantable patch antenna for ISM-band biomedical applications," *IEEE Trans. Antennas Propag.*, vol. 62, no. 5, pp. 2407–2417, 2014.

[6] D. Pinchera, M. D. Migliore, and F. Schettino, "An ultra wide permittivity antenna (UWPA) for reliable through-wall communications," *IEEE Trans. Antennas Propag.*, vol. 61, no. 2, pp. 957–960, 2013.

[7] M. Rad and L. Shafai, "Embedded microstrip patch antenna for structural health monitoring applications," in *International Symposium on Antennas and Propagation, APURSI*. IEEE, 2008, pp. 1–4.

[8] X. Jin and M. Ali, "Reflection and transmission properties of embedded dipoles and PIFAs inside concrete at 915 MHz," in *International Symposium on Antennas and Propagation, APURSI*. IEEE, 2009, pp. 1–4.

[9] S.-H. Jeong and H.-W. Son, "UHF RFID tag antenna for embedded use in a concrete floor," *IEEE Antennas Wirel. Propag. Lett.*, vol. 10, pp. 1158–1161, 2011.

[10] C. Thajudeen, A. Hoorfar, F. Ahmad, and T. Dogaru, "Measured complex permittivity of walls with different hydration levels and the effect on power estimation of TWRI target returns," *Progress In Electromagnetics Research B*, vol. 30, pp. 177–199, 2011.

[11] L. Kosuru and D. Deavours, "Optimum performance for RFID tag immersed in dielectric media," in *RFID (RFID), 2011 IEEE International Conference on*, April 2011, pp. 11–18.

[12] Y. Mushiake, "Self-complementary antennas," *IEEE Antennas Propag. Mag*, vol. 34, no. 6, pp. 23–29, 1992.

[13] S. Maddio, A. Cidronali, and G. Manes, "A new design method for single-feed circular polarization microstrip antenna with an arbitrary impedance matching condition," *IEEE Trans. Antennas Propag.*, vol. 59, no. 2, pp. 379–389, 2011.

[14] F. Abboud, J. Damiano, and A. Papiernik, "Simple model for the input impedance of coax-fed rectangular microstrip patch antenna for CAD," in *IEE Proceedings H (Microwaves, Antennas and Propagation)*, vol. 135, no. 5. IET, 1988, pp. 323–326.

[15] M. Deshpande and M. Bailey, "Input impedance of microstrip antennas," *IEEE Trans. Antennas Propag.*, vol. 30, no. 4, pp. 645–650, 1982.

[16] C. A. Balanis, *Antenna theory: analysis and design*. John Wiley & Sons, 2012.

[17] R. Garg and S. Long, "Resonant frequency of electrically thick rectangular microstrip antennas," *Electron. Lett.*, vol. 23, no. 21, pp. 1149–1151, 1987.

[18] R. Garg, *Microstrip antenna design handbook*. Artech House, 2001.

[19] J. R. James, P. S. Hall, and C. Wood, *Microstrip antenna theory and design*. IET, 1981, no. 12.

[20] R. Sorrentino and G. Bianchi, *Microwave and RF engineering*. John Wiley & Sons, 2010, vol. 1.

[21] K. Gupta, R. Garg, I. Bahl, and P. Bhartia, *Microstrip Lines and Slotlines*. Arthech House, 1996.

[22] J. Vandensande, H. Pues, and A. Van de Capelle, "Calculation of the bandwidth of microstrip resonator antennas," in *Microwave Conference, 1979. 9th European*. IEEE, 1979, pp. 116–119.

[23] I. Wolff and N. Knoppik, "Rectangular and circular microstrip disk capacitors and resonators," *IEEE Trans. Microw. Theory Techn.*, vol. 22, no. 10, pp. 857–864, 1974.

[24] J. J. Wang, Y. P. Zhang, K. M. Chua, and A. C. W. Lu, "Circuit model of microstrip patch antenna on ceramic land grid array package for antenna-chip codesign of highly integrated RF transceivers," *IEEE Trans. Antennas Propag.*, vol. 53, no. 12, pp. 3877–3883, 2005.